Correlated Shadow-Fading in Wireless Networks and its Effect on Call Dropping

Krishnan Kumaran, Steven E. Golowich, Sem Borst
Bell Laboratories, Lucent Technologies
600 Mountain Avenue, Murray Hill, NJ 07974

Abstract

We discuss a statistical model to generate correlated shadow-fading patterns for wireless systems in the absence of detailed propagation and landscape information. The currently available autocorrelation models result in anomalous effects that depend on traffic density and mobility, as they propose independent random processes for each mobile. Our approach involves generating a pre-computed fading map with the right marginal distributions and spatial correlations, which avoids inconsistencies such as providing widely differing values for mobiles close to each other. The correlations are introduced via a Gaussian random field, which has a covariance structure that depends on a set of parameters which can be computed from local measurements. The model is efficiently implemented using standard linear-algebra methods.

We conclude by describing a simulation experiment to study the effect of correlations on call dropping. The experiment reveals a strong relationship between call dropping and the correlation length of the fading pattern, and indicates circumstances under which dropping may be relatively high.

1 Introduction

Propagation is a crucial factor in the design and performance of wireless systems. There are several statistical methods to estimate propagation under different conditions, and most of these methods are computationally intensive. 2D and 3D ray tracing methods, for example, are popular techniques with much effort devoted to enhance their computational viability (see [2], [7] and references therein). Inaccuracies in modeling specific aspects of propagation, such as shadow-fading, could lead to distorted capacity and performance estimates in simulations and approximate analytical calculations. Shadow-fading is the slowly varying component of propagation that arises, as the name suggests, primarily from obstacles. Raleigh fading, which is a propagation variation on a smaller scale, is also an important factor for stationary or slow moving users of the wireless system, but we do not deal with it here.

For some applications, it is useful to have a statistical model of propagation with an empirical validity for the conditions of interest. It is in this spirit that the log-normal distribution, which is most widely used at the present, was proposed. In this model, the received power at each location is assumed to be independent of other locations and log-normally distributed about a deterministic large-scale decay, i.e.,

$$P(r) = P_0(r)\, e^s \tag{1}$$

where s is normally distributed with mean 0 and $\log P_0(r)$ is the average value of $\log P(r)$ received at distance r from the transmitter after large-scale fading. Usual forms for this function are $P_0(r) = A + B\,\log(r)$ (the Hata Model [5]) or simply the power law decay $P_0(r) = \dfrac{K}{r^d}$ where A, B, K and d are specific constants depending on the environment. While these models are simple and account for the observed marginal distributions, they fail to capture the spatial correlations inherent in shadow-fading, which cause its slowly-varying behavior. Simulations of wireless systems that ignore such spatial correlations could give seriously misleading results, as we illustrate below with an example of a call drop rate calculation.

Our interest in generating realistic shadow-fading patterns arose in the context of a simulation study of a novel Interference-Based Dynamic Channel Assignment algorithm [1]. The proposed algorithm relies on periodic interference measurements on the inactive frequencies so as to identify appropriate candidate channels. To obtain accurate estimates of the impact on system capacity and voice quality, we were confronted with the problem of generating shadow-fading values consistent with specified marginal distributions and correlation parameters.

The issue of capturing correlations in shadow-fading has been addressed previously by Gudmund-son [3, 4] by means of an auto-regressive model that approaches the issue differently. The correlations considered there are between the shadow-fading values seen by a mobile as it moves in the environment. In simulations, this would imply independent random processes for each mobile admitted to the network. Thus, one encounters anomalies such as the assignment of completely different shadow-fading values for different mobiles at nearby locations or at different times at the same location.

Our approach is to precompute a static, spatially correlated shadow-fading pattern with the desired statistical characteristics. The mobiles then acquire fading values as they move within the domain of the map, thus avoiding the inconsistencies mentioned above. The method is analytically tractable and computationally efficient. It is well suited for simulations that are aimed at obtaining performance characteristics not directly related to specific propagation aspects, but would benefit from using realistic fading models for generic environments.

Finally, we describe a simulation experiment designed to study the effect of correlations on call dropping, an important performance criterion for wireless networks. The experiment adopts a simple random walk mobility model for mobiles moving within a pattern produced using our fading model.

2 Description of the Model

Assume that we are given a 2D lattice representation of the region in which we are interested, with the positions of the lattice points denoted $x \in \mathbb{Z}^2$, and we restrict attention to the square sub-lattice $\Lambda = \mathbb{Z}^2 \cap [0, N-1]^2$ (it would be equally valid to use a polar grid with the appropriate local transformation of the coefficients*). We define the random field $\Xi(x)$, which describes the shadow-fading at position x, from which the received power is calculated as before.

$$P(x) = P_0(x)\, e^{\Xi(x)} \tag{2}$$

For shadow-fading, measurements available pertain to marginal variances and correlation lengths [3, 4]. In the absence of more detailed statistics on the shadow-fading patterns, we would like to choose the simplest possible model for Ξ that is capable of reproducing such measurements. We propose to model Ξ as a zero-mean Gaussian random field with a covariance structure that allows us to specify local variances and correlation lengths. A popular model in the spatial statistics literature is

$$C_{\Xi}(x, y) = \langle \Xi(x)\Xi(y) \rangle \simeq V(x) e^{-|x-y|/d(x)}, \tag{3}$$

where the local variance $V(x)$ and the local correlation length $d(x)$ are assumed to be slowly varying functions of position. The form (3) may also be generalized to allow different correlation lengths in different directions.

In general, the generation of such a Gaussian random field is a computationally expensive procedure for random fields large enough to be of practical interest. Hence, we choose a form for the covariance matrix for which fast algorithms exist to generate random fields, yet still approximates (3) well. The form we choose is

$$\Xi(x) = \sum_{y \in \Lambda} F(x, y)\, \phi(y), \tag{4}$$

*Polar coordinates would, in fact, be better suited to capture the radial nature of the propagation from a point source, by setting different correlation strengths along radial and tangential directions. The following analysis is however applicable to any coordinate system.

where $\phi(x)$ is a Gaussian random field with covariance given below and $F(x, y)$ is the smoothing filter

$$
\begin{aligned}
F(x, y) &= \sum_{z \in \Lambda} G(x, z)\, G(z, y) \\
G(x, y) &= \left(\frac{1}{2N(x) + 1} \right)^2 \mathbf{1}_{|x_i - y_i| \le N(x)}.
\end{aligned}
$$

Here $\mathbf{1}$ denotes the indicator function. We set $N(x) = d(x)/2$, which we have found yields a close agreement with (3). In the case that $d(x)$ is translationally invariant, the smoothing operation reduces to convolution with a hat function. The reasons for each of the two factors in the summand in (4) are as follows. The field $\phi(x)$ can be efficiently generated and its covariance, defined below, has the right long-distance behavior, but is too sharply peaked at short distances to approximate (3) well. This defect at short distances is remedied by the smoothing filter, which leaves the long-range behavior unaltered.

The Gaussian random field $\phi(x)$ is defined to have the probability density

$$
\mathrm{Prob}(\{\phi(x)\}) = (2\pi)^{-|\Lambda|/2} \det C_{\phi,\Lambda}^{-1/2} \exp \left(- \sum_{x,y \in \Lambda} \phi(x)\, C_{\phi,\Lambda}^{-1}(x, y)\, \phi(y) \right) \tag{5}
$$

where the inverse covariance matrix $C_{\phi,\Lambda}^{-1}(x, y)$ is given by

$$
\begin{aligned}
C_{\phi,\Lambda}^{-1}(x, y) &= \Lambda(x)\, C_{\phi}^{-1}(x, y)\, \Lambda(y) \\
C_{\phi}^{-1}(x, y) &= (\lambda I + \partial_1^T \mu_1 \partial_1 + \partial_2^T \mu_2 \partial_2)_{x,y}.
\end{aligned} \tag{6}
$$

Here I is the identity matrix, λ, μ_i are positive real-valued functions of the lattice position x, and ∂_i are the lattice difference operators defined by

$$
(\partial_i f)(x) = f(x + \mathbf{e}_i) - f(x),
$$

where $\mathbf{e}_i$ are unit vectors along the coordinate axes. We use the symbol Λ to denote both a subset of the lattice and the indicator function of the subset. Thus, $C_{\phi,\Lambda}^{-1}(x, y)$ is a restriction of the infinite-lattice operator $C_{\phi}^{-1}(x, y)$. We analyze the properties of these operators in the Appendix. In the case in which we are interested, of lattices that are large compared to the correlation lengths, $C_{\phi,\Lambda}$ differs from C_ϕ very little.

The covariance matrix for $\Xi(x)$ can be recovered from that of $\phi(x)$ via

$$
C_{\Xi}(x, y) = \sum_{v,w \in \Lambda} F(x - v)\, F(y - w)\, C_{\phi}(v, w). \tag{7}
$$

Because F is a short-range smoothing filter, the asymptotic decay of C_Ξ is the same as that of C_ϕ. Analytic approximations for the variance of Ξ can be obtained, but it happens that for lattice sizes of interest the approximations are poor. Hence in practice, the variances $C_\Xi(x,x)$ must be computed numerically, which we show below how to do.

The parameters $\lambda(x)$, $\mu_i(x)$ determine the covariances of the random fields $\phi(x)$ and $\Xi(x)$. In the special, but interesting, case of λ and μ_i constant, and $\lambda \ll \mu_i$, one can compute the asymptotic behavior (as $|x-y|$ becomes large) of $C_\phi(x,y)$ to be

$$C_\phi(x,y) \sim \frac{1}{2\sqrt{2\pi\mu_1\mu_2}} \frac{\exp\left(-\sqrt{\lambda}\left(\frac{(x_1-y_1)^2}{\mu_1}+\frac{(x_2-y_2)^2}{\mu_2}\right)^{1/2}\right)}{\lambda^{1/4}\left(\frac{(x_1-y_1)^2}{\mu_1}+\frac{(x_2-y_2)^2}{\mu_2}\right)^{1/4}}. \tag{8}$$

The calculation of (8) is sketched in the appendix. We see that the covariance matrix C_ϕ exhibits exponential decay, with correlation lengths $\sqrt{\mu_i/\lambda}$ along the coordinate axes. The condition $\lambda \ll \mu_i$ is a reasonable one for our purposes, since it is consistent with correlation lengths of at least a few lattice spacings.

From (7), we see that the behavior of $C_\Xi(x,y)$ is the same as that of $C_\phi(x,y)$ for large $|x-y|$; the short-range smoothing filter does not influence the long-range decay. The filter F does have a large effect on the short-range properties of C_Ξ, however. Of most interest to us is the variance $C_\Xi(x,x)$, which in the translationally invariant infinite-volume case is given by

$$C_\Xi(x,x) = \int_{[-\pi,\pi]^2} \frac{d^2k}{(2\pi)^2} D_N^2(k) \left(\lambda + 4\sum_{\alpha=1}^{2} \mu_\alpha \sin^2(k_\alpha/2)\right)^{-1} \tag{9}$$

where $D_N(k)$ is the Dirichlet kernel

$$D_N(k) = \frac{1}{(2N+1)^2} \prod_{\alpha=1}^{2} \frac{\sin(k_\alpha(2N+1)/2)}{\sin(k_\alpha/2)}. \tag{10}$$

Closed form analytic approximations to (9) can be obtained, but the approximations are poor in the cases of practical interest. Therefore we calculate the variances numerically, which we show how to do in finite volume in section 3.

When the functions $\lambda(x)$ and $\mu_i(x)$ are not constant, the expressions (8) and (9), along with the method of calculation, no longer hold. However, we show in the Appendix that if $\lambda(x)$ and $\mu_i(x)$ vary slowly compared to the correlation length, then $C_\Xi(x,y)$ will behave like (8) and (9) locally. In particular, $C_\Xi(x,y)$ will have exponential decay of the form (8), with correlation lengths given by the local values $\sqrt{\mu_i(x)/\lambda(x)}$, and the variance calculation (9) approximates the true local variance well.

Available measurements for shadow-fading include marginal distributions and correlation lengths. With the aid of (8) and numerical solutions to (9), one can fix the variance σ^2 and correlation lengths in the coordinate directions d_1, d_2 of $\phi(x)$ to match experimentally measured values.

3 Algorithms

We now discuss algorithms to generate numbers obeying the joint normal distribution (4). We use different methods depending on whether the parameters $\lambda(x)$, $\mu_i(x)$ are constant or not.

Constant parameters

In the Appendix, the Discrete Fourier Transform (DFT) is used to diagonalize the infinite-volume version of the covariance C_ϕ in order to compute (8), and we show how to recover the finite-volume covariance $C_{\phi,\Lambda}$ from C_ϕ. Of the various possibilities for restricting to finite volume, we have chosen to impose Dirichlet boundary conditions on the lattice Laplacians in (6). Other choices of boundary conditions, such as periodic or Neumann, are possible; the reader is referred to [GJ] for an explanation of how to use the method of images to recover the various finite-dimensional kernels corresponding to different choices of boundary conditions from the infinite-volume kernel.

One may use the Discrete Sine Transform (DST) to draw random fields $\Xi(x)$ with covariances given by $C_{\Xi,\Lambda}$. Because the DST can be implemented by the Fast Fourier Transform (FFT), this will result in a very efficient method for drawing random fields. $C_{\Xi,\Lambda}$ is diagonalized by the eigenvectors

$$\left\{ e_k(x) : k \in \frac{\pi}{N+1}\mathbb{Z}^2, 0 < k_\alpha < \pi \right\} \tag{11}$$

where $e_k(x)$ is defined by

$$\begin{aligned} e^{(1)}_{k_\alpha}(x_\alpha) &= \left(\frac{2}{N+1}\right)^{1/2} \sin(k_\alpha(x_\alpha+1)) \\ e_k(x) &= \prod_{\alpha=1}^{2} e^{(1)}_{k_\alpha}(x_\alpha). \end{aligned}$$

The spectrum $\hat{C}_{\Xi,\Lambda}(k)$ of $C_{\Xi,\Lambda}$ is given by

$$\hat{C}_{\Xi,\Lambda}(k) = D_N(k)\left(\lambda + 4\sum_{\alpha=1}^{2}\mu_\alpha \sin^2(k_\alpha/2)\right)^{-1}$$

where $D_N(k)$ is the Dirichlet kernel defined in (10). The matrix of eigenvectors (11) defines a unitary transform $U(x,k)$, the DST, which may be implemented by the FFT. We draw fields $\Xi(x)$ with covariance matrix

$C_{\Xi,\Lambda}(x,y)$ by first drawing N^2 iid random numbers $\psi(k)$ distributed normally, with mean 0 and variance 1. Then let

$$\Xi(x) = \sum_k U(x,k)\,\hat{C}^{1/2}_{\Xi,\Lambda}(k)\,\psi(k).$$

A calculation shows that $\langle \Xi(x)\Xi(y)\rangle = C_{\Xi,\Lambda}(x,y)$, as desired.

We stated above that the function relating the variances to the parameters λ, μ_i must be computed numerically. This may be efficiently accomplished using the equation

$$\begin{aligned} C_{\Xi,\Lambda}(x,x) &= \sum_k U(x,k)^2\,\hat{C}_{\Xi,\Lambda}(k) \\ &= \left(\frac{2}{N+1}\right)^2 \sum_k \sin^2(k_1x_1)\,\sin^2(k_2x_2)\,\hat{C}_{\Xi,\Lambda}(k). \end{aligned}$$

Variable parameters

If $\lambda(x)$, $\mu_i(x)$ vary with x, then the covariance $C_{\Xi,\Lambda}(x,y)$ will no longer be diagonalized by the DFT, and a different procedure must be followed. In this case, we first generate the fields $\phi(x)$, and then recover $\Xi(x)$ from $\phi(x)$ using (4).

We begin by rewriting the quadratic form in (5) in matrix notation as

$$\sum_{x,y\in\Lambda} \phi(x)C^{-1}_{\phi,\Lambda}(x,y)\phi(y) = \phi^{\mathbf{T}}\,\mathbf{A}\,\phi \tag{12}$$

where ϕ is a column vector containing all the ϕ_{ij}, i.e., $\phi_k = \phi_{(i+N),j} = \phi_{ij}$ or $\phi_k = \phi_{int(k/N),mod(k,N)}$ and A is a symmetric, block-tridiagonal matrix of the form

$$\mathbf{A} = \begin{pmatrix} \mathbf{A}_1 & \mathbf{D}_1^T & \mathbf{0} & \cdots \\ \mathbf{D}_1 & \mathbf{A}_2 & \mathbf{D}_2^T & \ddots \\ \mathbf{0} & \mathbf{D}_2 & \mathbf{A}_3 & \ddots \\ \vdots & \ddots & \ddots & \ddots \end{pmatrix}$$

The matrices $\mathbf{D}_i$ and $\mathbf{A}_i$ are given by

$$\mathbf{D}_i = \begin{pmatrix} -\mu^x_{i-1,1} & 0 & \cdots \\ 0 & -\mu^x_{i-1,2} & 0 \\ \vdots & 0 & \ddots \end{pmatrix},\ \mathbf{A}_i = \begin{pmatrix} \chi_{i1} & -\mu^y_{i1} & 0 \\ -\mu^y_{i1} & \chi_{i2} & \ddots \\ 0 & \ddots & \ddots \end{pmatrix}$$

where $\chi_{ij} = \lambda_{ij} + \mu^y_{i,j-1} + \mu^y_{ij} + \mu^x_{i-1,j} + \mu^x_{ij}$. We have imposed the boundary conditions $\mu_{ij} = 0$ for $i, j \leq 0$ or $i, j \geq N-1$. Several interesting mathematical properties of the specific distribution (5) are discussed in [6]. In particular, $\mathbf{A}$ is diagonally dominant and hence positive-definite, and its inverse consists of all positive entries.

The matrix $\mathbf{A}$, being symmetric and positive-definite, can be decomposed as

$$\mathbf{A} = \mathbf{L}\mathbf{L}^T \tag{13}$$

which is also referred to as taking the "square root" of the matrix $\mathbf{A}$ or as the Cholesky decomposition of $\mathbf{A}$. In our case, the block tridiagonal structure of $\mathbf{A}$ offers considerable computational advantages by breaking down equation (13) as

$$\mathbf{A} = \begin{pmatrix} \mathbf{L}_1 & \mathbf{0} & \dots & \dots \\ \mathbf{B}_1 & \mathbf{L}_2 & \ddots & \ddots \\ \mathbf{0} & \mathbf{B}_2 & \mathbf{L}_3 & \ddots \\ \vdots & \ddots & \ddots & \ddots \end{pmatrix} \begin{pmatrix} \mathbf{L}_1^T & \mathbf{B}_1^T & \mathbf{0} & \dots \\ \mathbf{0} & \mathbf{L}_2^T & \mathbf{B}_2^T & \ddots \\ \vdots & \ddots & \mathbf{L}_3^T & \ddots \\ \vdots & \ddots & \ddots & \ddots \end{pmatrix} \tag{14}$$

and the smaller individual sub-matrices are obtained using standard Cholesky decomposition as

$$\begin{aligned} \mathbf{L}_i\mathbf{L}_i^T &= \mathbf{A}_i - \mathbf{B}_{i-1}\mathbf{B}_{i-1}^T \\ \mathbf{B}_i &= \mathbf{D}_i\mathbf{L}_i^{-T} \end{aligned} \tag{15}$$

[†]This decomposition allows the change of variables $\psi = \mathbf{L}^T\phi$ and it is readily verified that the variables ψ_{ij} are uncorrelated univariate Gaussians with mean 0. Thus the ϕ_{ij} can be obtained by inversion as $\phi = \mathbf{L}^{-T}\psi$. Again, the inversion can be performed more efficiently than in the case of general covariances by using the special structure of the matrix as $\mathbf{L}_i^T\phi_i = \psi_i - \mathbf{B}_i^T\phi_{i+1}$. Given the matrix $\mathbf{A}$, the algorithm to generate the distribution is hence summarized as follows.

- Perform the decomposition (15) and store the matrix $\mathbf{L}^T$.

[†]The superscript $-T$ stands for the inverse of the transpose.

- Generate the independent Gaussian variables ψ_{ij} with mean 0 and variance 1. This may be performed by several methods using the standard uniform random-number generators in the range $[0,1]$. A simple and efficient option is the cosine method which involves generating pairs of uncorrelated Gaussian variables ψ_1 and ψ_2 using the uniform variables u_1 and u_2 as

$$\begin{aligned}\psi_1 &= \sqrt{-2\ln u_1}\cos 2\pi u_2\\ \psi_2 &= \sqrt{-2\ln u_1}\sin 2\pi u_2\end{aligned}$$

- Apply $\mathbf{L}^{-T}$ to the vector ψ to obtain ϕ.

- Apply the smoothing filter F to ϕ to obtain Ξ, as in (4).

Note that successive samples ϕ can be generated by simply applying the inverse of the stored upper triangular matrix $\mathbf{L}^T$ to a different ψ, which can be performed with much greater computational efficiency than the first sample.

4 Multiple Base Stations

It is expected that the powers received at a given point from two different base stations are correlated, because of correlations in the landscape. This correlation depends on the positions of the two base stations relative to the position of the mobile unit. Therefore, the Gaussian random fields associated with the various base stations should be correlated. We would like to specify the correlation structure

$$\begin{aligned}\langle \Xi_i(x)\Xi_i(y)\rangle &= C_\Xi(x,y)\\ \langle \Xi_i(x)\Xi_j(x)\rangle &= f_{ij}(x)C_\Xi(x,x)\end{aligned} \tag{16}$$

where Ξ_i is the field associated with the i^{th} base station, and $f_{ij}(x) = f_{ji}(x)$ are functions that are slowly varying on the scale of the correlation length of C_Ξ. The meaning of (16) is that each of the various fields Ξ_i associated with the different base stations is correlated with itself according to the covariance $C_\Xi(x,y)$ developed earlier, while the correlations between the fields of two different base stations at the same point x are specified by the functions $f_{ij}(x)$. We are not concerned with correlations between the fields of different base stations at different points, since we only apply such correlations to a single mobile at a time.

We assume that the $f_{ij}(x)$ obey the bounds

$$|f_{ij}(x)| \leq 1 \qquad \forall\, i,j,x$$

$$\sum_{j \neq i} |f_{ij}(x)| \quad \leq \quad 1 \qquad \forall\, i, x. \tag{17}$$

The second requirement will not prove very restrictive for us because we are only interested in these correlations for the purposes of analyzing handoff. Hence we may choose $f_{ij} \equiv 0$ unless i and j are nearest neighbors. Also, only two or three base stations are involved in hand-offs, so if x is in a handoff region at most three of the f_{ij} need have appreciable values. We give examples below.

We will define Gaussian random fields that approximately satisfy (16) and can be efficiently generated. The approximation improves as the correlation length of C_Ξ decreases and as the functions f_{ij} become more slowly varying. To begin, draw a number of iid random fields $\{\Psi_{ij}\}$, one for each f_{ij} that is not identically zero, all with covariance structure $C_\Xi(x, y)$ (there are at most $\binom{N}{2}$ such fields). Define $\Psi_{ji} = \Psi_{ij}$. Then draw N more iid fields $\{\tilde{\Xi}_i\}_{i=1\ldots N}$ with the same covariance structure. Define

$$\Xi_i(x) = \sum_{j \neq i} \delta_{ij}(x) |f_{ij}(x)|^{1/2} \Psi_{ij}(x) + \left(1 - \sum_{j \neq i} |f_{ij}(x)|\right)^{1/2} \tilde{\Xi}_i(x)$$

where

$$\delta_{ij} = \begin{cases} \mathrm{sign}(f_{ij}(x)) & \text{if } i < j \\ 1 & \text{otherwise} \end{cases}$$

Our assumptions on f_{ij} imply that $f_{ij}(x) \simeq f_{ij}(y)$ for $|x - y| < \xi$. Using this approximation, along with the independence of the different fields, it is easy to see that the correlation structure of the Ξ_i approximates (16).

We end with an example of a reasonable choice of functions $f_{ij}(x)$. We choose the f_{ij} to be functions of $\theta_{ij}(x)$, the angle between the vectors from base stations i and j to x. One would expect the received power from the two base stations to be least correlated when $\theta_{ij}(x)$ is close to π, and most correlated when it is close to 0. Also, recall that we are only interested in this type of correlation when a mobile is in a handoff region. This leads us to the definition

$$f_{ij}(x) = \Gamma_{ij}(x)\, \tilde{f}_{ij}(x)$$

where $\Gamma_{ij}(x)$ is a function that is 1 in a region in which hand-offs between i and j are likely to occur and tends smoothly to zero outside of this region (see figure 1), and

$$\tilde{f}_{ij}(x) = g\left(\epsilon + (1 - \epsilon)\frac{1 + \cos\theta_{ij}(x)}{2}\right). \tag{18}$$

Here $g, \epsilon \in [0, 1]$, with ϵ small and g close to 1. The reason for the Γ_{ij} factor is to ensure that (17) is satisfied. At most three Γ_{ij} take the value 1 at the same point (for reasonable locations of the base stations), corresponding to at most three base stations involved in handoff. (17) is trivially satisfied at positions where only two Γ_{ij}

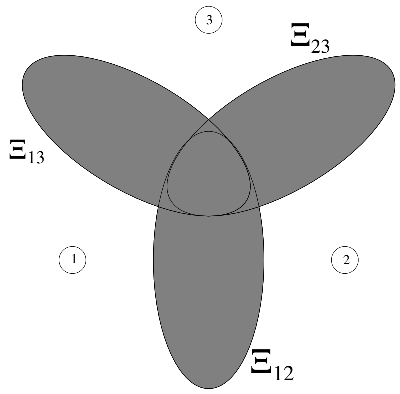

Figure 1: Correlated fields associated with multiple base stations. The Γ_{ij} are identically 1 in the shaded regions, and fall off smoothly to 0 outside of these regions. The area where any three Γ_{ij} are identically 1 is typically confined to the interior of the triangle defined by the three base stations.

are nonzero. When three base stations are involved, we note that the regions of three overlapping $\Gamma_{ij} = 1$ will be confined to the triangle defined by the three base stations, and with this it is not hard to see that (17) will be satisfied.

5 Numerical Experiments

We now describe a simulation experiment to investigate the effect of correlations on call dropping, which is an important performance criterion in wireless networks. In fact, call dropping, which refers to interruption of a call in progress, is generally considered a more serious performance failure than blocking admission to a new call, and hence is usually required to be below 1% for adequate performance.

We performed the following experiment to demonstrate the effect of correlations on call dropping. Consider a region in the coverage area sufficiently distant from the antenna so that the large scale propagation path loss is approximately constant within the region, and hence the only macroscopic fluctuations in received signal come from shadowing. As mentioned before, we ignore the smaller scale fluctuations due to Rayleigh fading.

For this region, we produce the shadow-fading pattern using the Gaussian random field method described earlier, followed by the imposition of a tolerance threshold to distinguish regions with weak and strong signal. This produces a pattern of the type shown in Figure 4, where gray represents strong signal and black represents shadow. The mobile trajectories, shown in white, are then random walks within the region generated as follows. The initial location is generated uniformly within the central portion of the square region R to reduce the

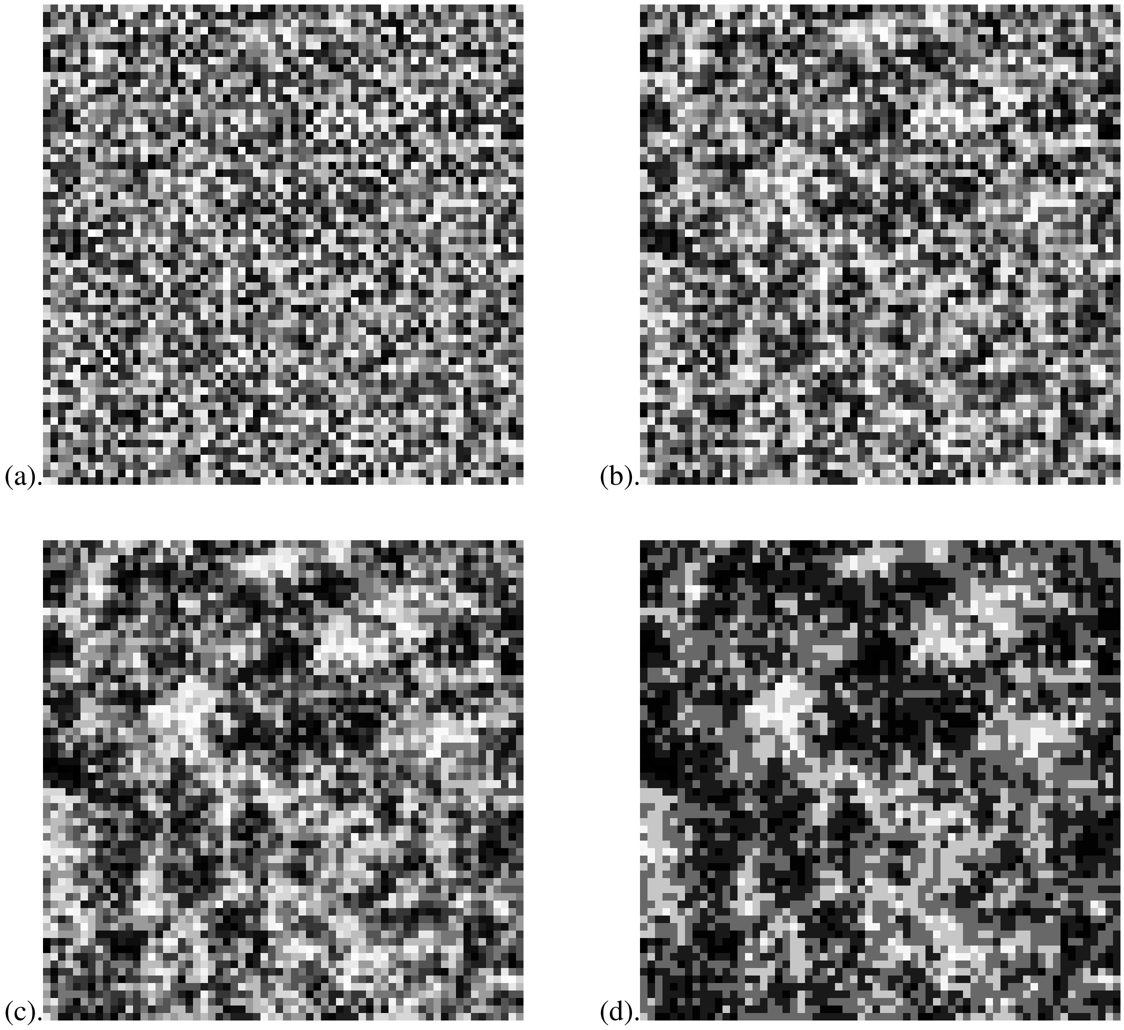

Figure 2: (a) Uncorrelated Gaussian pattern. (b) through (d) - Increasing correlation strengths produce more clustered patterns from (a).

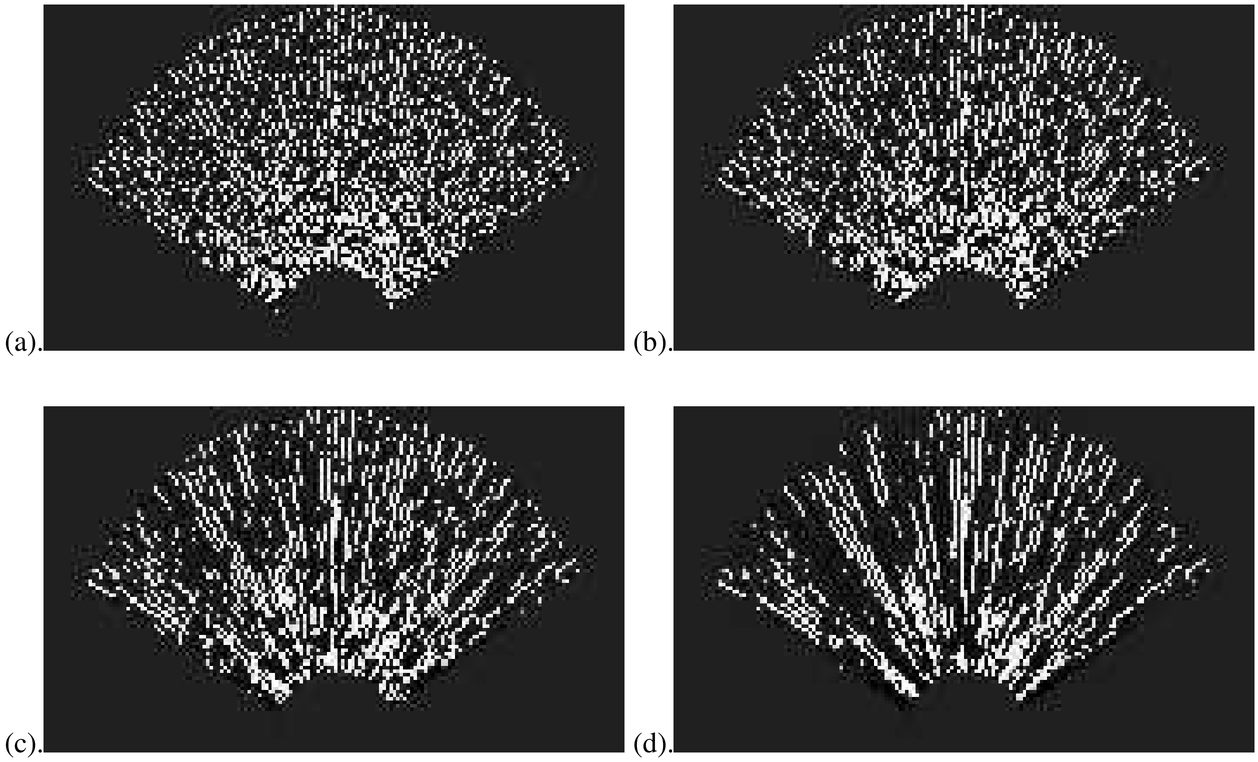

Figure 3: (a) Uncorrelated Radial pattern. (b) through (d) - Increasing radial correlation strengths shadow out certain sections along each radial line, while the remaining regions receive a stronger signal.

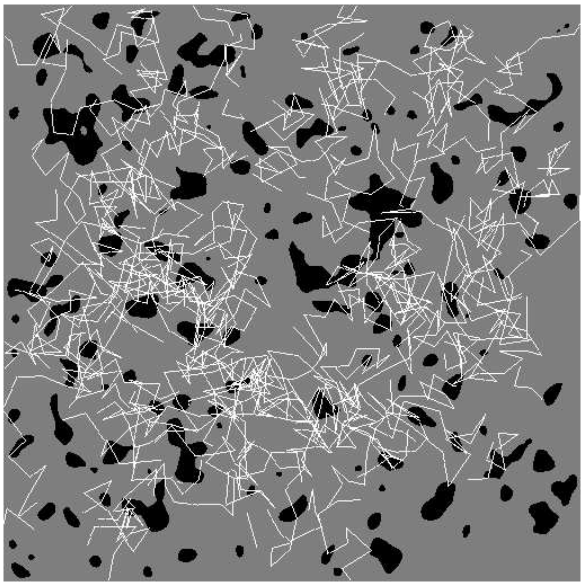

Figure 4: Typical shadowing pattern used in the experiment, with sample trajectories of mobiles depicted in white.

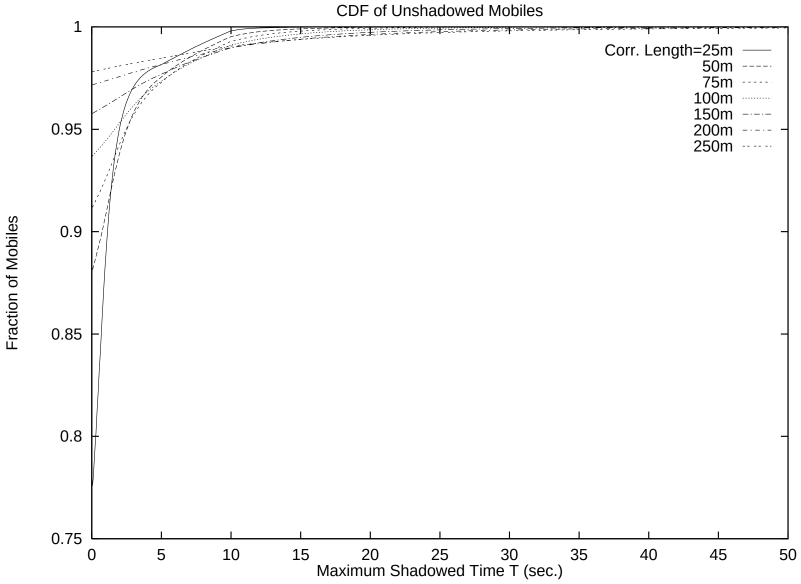

Figure 5: Distribution function of maximum shadowed time of mobiles for various correlation lengths.

chances of mobiles wandering out of the region. If the initial position falls in a shadowed area, the mobile is immediately discarded. During their lifetime, which is exponentially distributed with mean 100s, the mobiles move along piecewise straight segments, making abrupt and random turns every so often. Each lattice spacing was taken to be 5 meters, with the pattern being 512x512 or 2.56 km x 2.56 km.

Denote by α_{mn}, T_{mn}, and V_{mn} the direction, the duration, and the velocity associated with the n-th segment of the trajectory of the m-th mobile. The α_{mn}'s are uniform on $[0, 2\pi]$, the T_{mn}'s are uniform on $[5, 10]sec$, and the V_{mn}'s are uniform on $[2, 6]\ spacings = [10, 30]m/s = [22.5, 67.5]mph$. All these random variables are mutually independent. The trajectory of a mobile is truncated when it dies or when it is about to leave the square region R, whichever occurs first.

For each mobile m, we keep track of the quantity Z_m, which is the maximum amount of time during which the mobile continuously experiences insufficient signal strength. This distribution is shown in figure 5 for various correlation lengths. We assume that dropping occurs if a mobile suffers from inadequate signal strength for more than θ consecutive time units. Thus $D_\theta = \Pr\{Z_m > \theta\}$ is the fraction of call dropping. Figure 6 depicts the dependence of dropping on correlation length for various values of θ.

Notice that the dropping curve for any fixed θ displays a "resonance"-like behavior, i.e. peaks at a critical correlation length. This qualitative behavior may be explained as follows. During a time period τ, a mobile traverses a certain number of unit bins (for our parameter values about 10). For dropping to occur, the signal

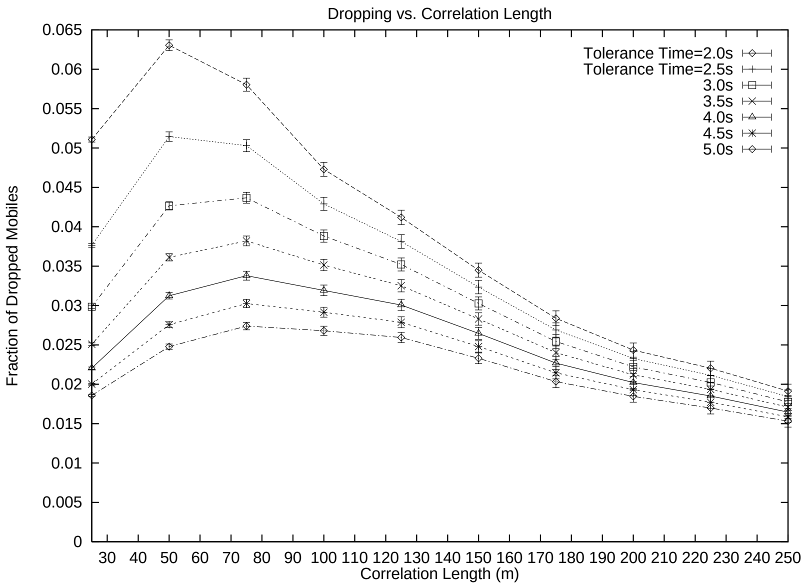

Figure 6: Call dropping as a function of correlation length for different tolerance intervals.

strength must be insufficient in all these bins. The probability of this event is quite low if the shadow-fading values in the successive bins are completely independent, and gradually increases with increasing correlation. However, increasing the correlation beyond a certain limit would not result in additional dropped calls, but instead fewer mobiles would experience longer shadowed times, driving the dropping rate down. Further, the peak appears around the value $d^* = \bar{V}\theta$, where $\bar{V} = 4\,spacings = 20m/s$ is the average speed of the mobile.

Thus, this experiment shows that it is critical to capture spatial correlations when studying the call dropping performance of a wireless network. However, this phenomenon cannot be controlled easily in a real network, where users usually have very diverse mobility patterns and θ is usually determined by link requirements. Also, shadowing patterns can vary in statistical characteristics within a real network. These factors suggest that certain user groups in certain locations could suffer greater call dropping than others, resulting in imbalanced service.

6 Conclusion

Sample patterns generated by our method with translationally invariant parameters are shown in figures 2 and 3. The typical size of the dark regions, controlled by the correlation lengths, are meant to reflect the typical size scale of obstacles in the environment. This crude property, although unconnected with the physics of propagation, is nevertheless useful in obtaining more realistic performance results from wireless simulations not committed to a specific propagation environment, such as the one described in [1]. This fact was observed in an actual wireless simulation effort, and is also suggested by our experiment to demonstrate the effect of correlations on call dropping. Other performance measures that could potentially be affected by correlations include inter-cell and intra-cell hand-over rates and variations in carrier-to-interference-ratio (C/I), which is an indicator of call quality.

The computational efficiency and the off-line nature of our algorithm to generate the patterns can help speed up simulations. The values generated have consistent statistical properties, and are not affected by mobility, as autocorrelation models are. However, additional memory is required to store the patterns generated, which limits the admissible grid size/resolution.

Much work needs to be done, however, in order to enhance the model based on physical arguments. The variances and correlation lengths, which we assume to be empirically set parameters, require justification from the physics of propagation, which may then serve as a means to estimate them. Such enhancements could, in the long term, save on computational and measurement efforts involved in designing and operating intelligent wireless networks that respond satisfactorily to the uncertainties of propagation.

A Appendix

The results in this appendix apply only to the fields $\phi(x)$ with covariances $C_\phi(x,y)$ and $C_{\phi,\Lambda}(x,y)$, not to the fields $\Xi(x)$. For simplicity, we will drop the ϕ subscript throughout the appendix.

Translationally Invariant Covariances

We first sketch the proof of (8), which is the asymptotic behavior of the covariance matrix defined in (6). Lattice differences are translationally invariant, so we may diagonalize C by means of the Discrete Fourier Transform (DFT). One may easily compute the spectrum of C^{-1}, and hence invert the DFT to get a representation of the kernel as the Fourier integral

$$\begin{aligned} C(x,y) \quad = \quad C(x-y) \quad &= \int_{[-\pi,\pi]^2} \frac{d^2k}{(2\pi)^2} \frac{e^{ik\cdot(x-y)}}{D(k)} \\ D(k) \quad &= \lambda + 4\sum_{\alpha=1}^{2} \mu_\alpha \sin^2(k_\alpha/2) \end{aligned} \tag{19}$$

We will show below that this covariance exhibits exponential decay. We are interested in the parameter regime where the decay extends over at least a few lattice points. We will see that in this case the approximation $\lambda \ll \mu_1, \mu_2$ is reasonable. With this approximation, the long-distance behavior of $C(x-y)$ is given by (8).

This result is easiest to see when $x - y$ lies along a coordinate direction, say $\mathbf{e}_1$. The integrand in (19) is periodic in $\Re k_1$ and is a meromorphic function of k_1 for all $k_2 \in [-\pi, \pi]$, with two simple poles at

$$\Re k_1 = 0, \quad \Im k_1 = \pm \log(A + \sqrt{A^2 - 1})$$

where $A = 1 + (\lambda + 2\mu_2(1 - \cos(k_1))/2\mu_1)$. Hence we may deform the k_1 contour up or down to ∞, depending on the sign of $x_1 - y_1$, picking up the residue at the appropriate pole. Using our approximation $a \ll \mu_i$, we are left with the remaining integral

$$C(x-y) \simeq \frac{1}{2\sqrt{\mu_1 \mu_2}} \int_{-\pi}^{\pi} \frac{dk_2}{2\pi} \frac{\exp\left(-\left(\frac{\lambda}{\mu_1} + k_2^2\right)^{1/2} |x_1 - y_1|\right)}{\left(\frac{\lambda}{\mu_1} + k_2^2\right)^{1/2}}$$

which has the asymptotic behavior of (8), evaluated along the $\mathbf{e}_1$ axis.

The case of general $x - y$ is somewhat more involved, but similar. We outline the calculation, which follows that for the continuum operator [GJ] but is complicated by the presence of the lattice. Begin by making the change of variables $k_i \to k_i/\sqrt{\mu_i}$. Then write

$$k = k_{||}\hat{z} + k_{\perp}\hat{p}$$

where $\hat{z}$ is a unit vector along the direction $(x_1/\sqrt{\mu_1}, x_2/\sqrt{\mu_2})$, and $\hat{p} \perp \hat{z}$. We wish to change variables in our integral to one over $k_{||}$ and $k_{\perp}$ in a rectangle, which we may do as long as there exists some period T such that $T\hat{z} = 0 \bmod 2\pi(\sqrt{\mu_1}, \sqrt{\mu_2})$, which happens iff μ_2/μ_1 is rational. This is not restrictive because $C(x-y)$ is a continuous function of the μ_i.

Our integral is now of the form

$$C(x-y) = \int_{-k_{\perp}^{\max}}^{k_{\perp}^{\max}} \frac{dk_{\perp}}{2\pi} \int_{-k_{||}^{\max}}^{k_{||}^{\max}} \frac{dk_{||}}{2\pi} \frac{\exp\left(ik_{||}\left(\frac{(x_1-y_1)^2}{\mu_1} + \frac{(x_2-y_2)^2}{\mu_2}\right)^{1/2}\right)}{D(k_{||}\hat{z} + k_{\perp}\hat{p})}$$

where $k_{||}^{\max}$, $k_{\perp}^{\max}$ depend on μ_i and $x - y$. The integrand is a periodic function of $\Re k_{||}$, with period T, for all $k_{\perp} \in [-k_{\perp}^{\max}, k_{\perp}^{\max}]$, so we may again shift the $k_{||}$ contour up or down, in order to exhibit the exponential decay. The situation is complicated by the fact that there are now many poles to consider. In the case of $\lambda \ll \mu_i$ we can find a closed-form approximate solution by shifting the contour only a small distance ϵ from the origin, but still beyond the poles closest to the real axis, which are located at

$$\begin{aligned} \Re k_{||} &= n\frac{T}{M} \\ \Im k_{||} &= \pm\sqrt{\lambda + (k_{\perp} + nk_{\perp}^{\max})^2}. \end{aligned}$$

where n is any integer small enough that $|\Im k_{||}^*| < \epsilon$, and M is the number of times the contour $t\hat{z}$, $t \in [0,T]$ winds around the torus $[-\sqrt{\mu_i}\pi, \sqrt{\mu_i}\pi]^2$. Let $\bar{n}$ denote the largest allowed n in magnitude. The residues associated with these poles are responsible for the asymptotic behavior of $C(x-y)$, while the remaining integral can be shown to be a small correction. The sum of $dk_\perp$ integrals over the residues resulting from the $dk_{||}$ integral takes the form

$$C(x-y) = \frac{1}{2\sqrt{\mu_1\mu_2}} \int_{-\bar{n}k_\perp^{\max}}^{\bar{n}k_\perp^{\max}} \frac{dk_\perp}{2\pi} \frac{\exp\left(\sqrt{\lambda + k_\perp^2}\left(\frac{(x_1-y_1)^2}{\mu_1} + \frac{(x_2-y_2)^2}{\mu_2}\right)^{1/2}\right)}{\sqrt{\lambda + k_\perp^2}}$$

which results in the asymptotics (8).

We have worked in infinite volume throughout. One can calculate the kernels of these operators restricted to finite volume, with various choices of boundary conditions, by summing copies of the infinite-volume covariance by use of the method of images. Here we state the result for Dirichlet boundary conditions. Fix some $y \in \Lambda$. Let $\{y_j\}$ denote the infinite set of points that both contains y and is invariant under reflection about any of the edges of Λ. Let ϵ_j denote the number of reflections required to obtain y_j from y. Then it follows from uniqueness [GJ] that

$$C_{\phi,\Lambda}(x,y) = \sum_{j=0}^{\infty} (-1)^{\epsilon_j} C(x, y_j). \tag{20}$$

We learn from (20) that, if x and y are no closer than L to the boundary of Λ, then $|C_{\phi,\Lambda}(x,y) - C(x-y)| < O(e^{-2L/d})$, where d is the larger of the correlation lengths. Hence, if Λ is large compared to the correlation lengths, then away from the boundary $C_{\phi,\Lambda}$ behaves very much like C.

Non-Translationally Invariant Covariances

If $\lambda(x)$ or $\mu_i(x)$ vary with x, then the DFT no longer diagonalizes the covariance and the above method of computing the covariance matrix elements fails. In our application the functions $\mu_i(x)$ and $a(x)$ are slowly varying with lattice position x. In this case, the covariance $C(x,y)$ *locally* behaves like the translationally invariant covariance

$$\tilde{C} = (\tilde{\lambda} I + \partial_1^* \tilde{\mu}_1 \partial_1 + \partial_2^* \tilde{\mu}_2 \partial_2)^{-1}_{x,y}$$

where $\tilde{\mu}_i = \mu_i(x)$ and $\tilde{\lambda} = \lambda(x)$ are constants. As a consequence, $C(x,y)$ will have exponential decay at the rate given by the local values of $\mu_i(x)$, $\lambda(x)$. We summarize this behavior as

Theorem A.1 *Fix $x \in \mathbb{Z}^2$, and choose some $K > 0$. Let $\Gamma_r(x) = \{y \in \mathbb{Z}^2 : |y-x| \le r\}$. If the conditions*

$$(1 - \epsilon/N(x)) \le \left\{\frac{\lambda(w)}{\lambda(x)}, \quad \frac{\mu_i(w)}{\mu_i(x)}\right\} \le (1 + \epsilon/N(x)) \qquad \forall\, w \in \Gamma_{(N+K)/2}(x) \tag{21}$$

$$\sup_{\substack{i \\ z\in\Gamma_{(N+K)/2}(x) \\ y\in\Gamma_1(z)}} \frac{4\mu_i(y)}{\lambda(z)+\sum_{j=1}^2(\mu_i(z)+\mu_i(z-e_i))} \leq 1-\delta(x) \tag{22}$$

are satisfied, where $\delta(x) > 0$ *for all* x, $\underline{\delta} = \inf_{x\in\mathbb{Z}^2}\delta(x)$, *and*

$$N(x) = \frac{\log(\underline{\delta}\epsilon) - K\sqrt{\frac{\lambda(x)}{\min(\mu_1(x),\mu_2(x))}}}{\log(1-\delta(x))} \tag{23}$$

then

$$C(x,y) = \tilde{C}(x-y)(1+E(x,y))$$

where $|E(x,y)| < O(\epsilon)$ *for all* $y \in \Gamma_K(x)$. *In particular,* $C(x,y)$ *has the same exponential decay as* $\tilde{C}(x-y)$.

Proof. The idea of the proof is to compare the random walk representations of C and $\tilde{C}$. If the functions μ_i and a are slowly varying, then the most important terms of these representations for C and $\tilde{C}$ will nearly coincide, which implies that the two series nearly coincide.

To make this precise, we develop the random walk representation of $C(x,y)$ [GJ]. Write

$$\begin{aligned}\sum_{i=1,2}(\partial_i^*\mu_i\partial_i)_{x,y} &= \sum_{i=1,2}(\mu_i(x)+\mu_i(x-e_i))\mathbf{1}_{\{y=x\}} - \mu_i(x)\mathbf{1}_{\{y=x+e_i\}} - \mu_i(y)\mathbf{1}_{\{y=x-e_i\}} \\ &= D_{x,y} - J_{x,y}\end{aligned}$$

where D is the diagonal part and J is the off-diagonal part, which has nonzero entries only when x and y are nearest neighbors. We then define $\Lambda_{x,y} = D_{x,y} + \lambda(x)\mathbf{1}_{\{y=x\}}$, and expand $C(x,y)$ in the geometric series

$$\begin{aligned}C(x,y) &= (\Lambda - J)^{-1}_{x,y} \\ &= \Lambda^{-1}_{x,x}\sum_{n=0}^{\infty}(J\Lambda^{-1})^n_{x,y} \\ &= \sum_{\omega:x\to y}\beta(\omega)\end{aligned}$$

In the final equality, the sum is over all nearest-neighbor walks ω from x to y. The weights $\beta(\omega)$ are given by

$$\beta(\omega) = \Lambda^{-1}_{\omega(0),\omega(0)}J_{\omega(0),\omega(1)}\Lambda^{-1}_{\omega(1),\omega(1)}J_{\omega(1),\omega(2)}\cdots J_{\omega(N-1),\omega(N)}\Lambda^{-1}_{\omega(N),\omega(N)}$$

for an N-step walk ω. This expansion is convergent as long as $\|J\Lambda^{-1}\| < 1$. The operator norm is bounded above by the L_1–L_∞ norm of the kernel, so a sufficient condition is

$$\sup_x \Lambda^{-1}_{xx}\sum_{|y-x|=1}|J_{x,y}| < 1$$

which is insured by (22). Split this into long and short walks

$$\begin{aligned} C(x,y) &= \sum_{\substack{\omega:x\to y\\ |\omega|<N(x)}} \beta(\omega) + \sum_{\substack{\omega:x\to y\\ |\omega|\geq N(x)}} \beta(\omega) \\ &= C_{<N}(x,y) + C_{\geq N}(x,y) \end{aligned} \tag{24}$$

with $N(x)$ given in (23). We may bound the contribution from long walks as

$$\begin{aligned} C_{\geq N(x)}(x,y) &\leq \sum_{n=N(x)}^{\infty} N_{x\to y}(n) \sup_{|\omega|=n} \beta(\omega) \\ &\leq \Lambda_{y,y}^{-1} \sum_{n=N(x)}^{\infty} 4^n \sup_{\substack{|\omega|=n\\ \omega:x\to y}} \prod_{i=1}^{n} \frac{J_{\omega(i)\omega(i+1)}}{\Lambda_{\omega(i)\omega(i)}} \\ &\leq \Lambda_{y,y}^{-1} \sum_{n=N(x)}^{\infty} 4^n \left[\sup_{\substack{i\\ z\in\Gamma_{(N(x)+K)/2}(x)\\ y\in\Gamma_1(z)}} \frac{\mu_i(y)}{\Lambda_{zz}} \right]^{N(x)} \left[\sup_{\substack{i\\ z\in\mathbb{Z}^2\\ y\in\Gamma_1(z)}} \frac{\mu_i(y)}{\Lambda_{zz}} \right]^{n-N(x)} \\ &\leq \Lambda_{y,y}^{-1} \sum_{n=N(x)}^{\infty} (1-\delta(x))^{N(x)} (1-\underline{\delta})^{n-N(x)} \\ &\leq \frac{(1-\delta(x))^{N(x)}}{\underline{\delta}\Lambda_{y,y}}. \end{aligned}$$

Here we have used that the number $N_{x\to y}(n)$ of walks from x to y in n steps is bounded above by 4^n in two dimensions. The reason for the definition (23) of $N(x)$ is that, using our assumption of slow decay, we know that

$$\tilde{C}(x-y) \geq C_0 \exp\left(-K\sqrt{\frac{\lambda}{\min(\mu_1,\mu_2)}}\right) \quad \forall\, y \in \Gamma_K(x)$$

for some constant $C_0 = O(1)$. Therefore,

$$C_{\geq N(x)}(x,y) < O(\epsilon)\tilde{C}(x-y). \tag{25}$$

Note that we can also expand $\tilde{C}(x-y)$ in the same way, and the same argument implies that

$$\tilde{C}_{\geq N}(x,y) < O(\epsilon)\tilde{C}(x-y). \tag{26}$$

To handle the main term, we write

$$C_{<N}(x,y) = \sum_{\substack{\omega:x\to y\\ |\omega|<N}} \left(\frac{\beta(\omega)}{\tilde{\beta}(\omega)}\right) \tilde{\beta}(\omega)$$

where $\tilde{\beta}$ are the expansion weights for $\tilde{C}(x-y)$. The condition (21) on the variation in the parameters implies that

$$\frac{\beta(\omega)}{\tilde{\beta}(\omega)} = 1 + E'(\omega) \tag{27}$$

where $|E'(\omega)| < O(\epsilon)$ for all $y \in \Gamma_K(x), \omega : x \to y$. Therefore, we can write

$$C(x, y) = \tilde{C}(x - y)(1 + E(x, y))$$

with

$$E(x, y) = \frac{1}{\tilde{C}(x - y)} \left(\sum_{\substack{\omega : x \to y \\ |\omega| < N}} E'(\omega)\tilde{\beta}(\omega) + C_{\geq N}(x, y) - \tilde{C}_{\geq N}(x - y) \right)$$

From (25), (26), and (27), we see that we are done. ∎

References

[1] S.C. Borst, S.A. Grandhi, C.L. Kahn, K. Kumaran, B.D. Lubachevsky, and D. Sand. Wireless Simulation and Self-Organizing Spectrum Management. *Bell Labs Technical Journal*, 2(3):81–98, Summer 1997.

[2] S.J. Fortune, D.M. Gay, B.W. Kernighan, O. Landron, R.A. Valenzuela, and M.H. Wright. WISE Design of Indoor Wireless Systems: Practical Computation and Optimization. *IEEE Computational Science & Engineering*, 2(1):58–68, Spring 1995.

[3] M. Gudmundson. Analysis of Hand-over Algorithm. In *41st IEEE Transactions on Veh. Tech. Conf.*, pages 537–542, 1991.

[4] M. Gudmundson. Correlation Model for Shadow Fading in Mobile Radio Systems. *Electronics Letters*, 27(23):2145–2146, November 1991.

[5] M. Hata. Empirical Formula for Propagation Loss in Land Mobile Radio Services. *IEEE Transactions on Vehicular Technology*, 29:317–325, 1980.

[6] K. Kumaran, D. Geiger, and L. Gurvits. Illusory surfaces and visual organization. *Network: Computation in Neural Systems*, 7(1):33–60, February 1996.

[7] A. Rajkumar, B.F. Naylor, F. Feisullin, and L. Rogers. Predicting RF coverage in Large Environments using Ray-Beam Tracing and Partitioning Tree Represented Geometry. *Wireless Networks*, 2(2):143–154, June 1996.